Journal of
www. biophotonics-journal.org
BIOPHOTONICS

FULL ARTICLE

# Versatile laser-based cell manipulator

*Nicola Maghelli and Iva M. Tolić-Nørrelykke*

[1] Max-Planck-Institute of Molecular Cell Biology and Genetics, 01307 Dresden, Germany

Received 13 April 2008, revised 4 June 2008, accepted 10 June 2008
Published online 14 July 2008

**Key words:** Nonlinear, laser ablation, optical tweezer, Two-photon

Here we describe a two-photon microscope and laser ablation setup combined with optical tweezers. We tested the setup on the fission yeast *Schizosaccharomyces pombe*, a commonly used model organism. We show that long-term imaging can be achieved without significant photo-bleaching or damage of the sample. The setup can precisely ablate sub-micrometer structures, such as microtubules and mitotic spindles, inside living cells, which remain viable after the manipulation. Longer exposure times lead to ablation, while shorter exposures lead to photo-bleaching of the target structure. We used optical tweezers to trap intracellular particles and to displace the cell nucleus. Two-photon fluorescence imaging of the manipulated cell can be performed simultaneously with trapping. The combination of techniques described here may help to solve a variety of problems in cell biology, such as positioning of organelles and the forces exerted by the cytoskeleton.

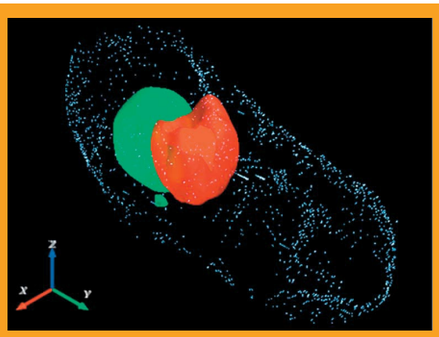


Three-dimensional representation of a cell where the nucleus was displaced using optical tweezers. The nucleus before the manipulation is displayed in red, and after the manipulation in green. The white dots show the cell volume.

J. Biophoton. 1, No. **4**, 299–309 (2008) / **DOI** 10.1002/jbio.200810026

J. Biophoton. **1**, No. 4, 299–309 (2008) / **DOI** 10.1002/jbio.200810026

Journal of BIOPHOTONICS

FULL ARTICLE

# Versatile laser-based cell manipulator

*Nicola Maghelli* and Iva M. Tolić-Nørrelykke*

[1] Max-Planck-Institute of Molecular Cell Biology and Genetics, 01307 Dresden, Germany

Received 13 April 2008, revised 4 June 2008, accepted 10 June 2008
Published online 14 July 2008

**Key words:** Nonlinear, laser ablation, optical tweezer, Two-photon

Here we describe a two-photon microscope and laser ablation setup combined with optical tweezers. We tested the setup on the fission yeast *Schizosaccharomyces pombe*, a commonly used model organism. We show that long-term imaging can be achieved without significant photo-bleaching or damage of the sample. The setup can precisely ablate sub-micrometer structures, such as microtubules and mitotic spindles, inside living cells, which remain viable after the manipulation. Longer exposure times lead to ablation, while shorter exposures lead to photo-bleaching of the target structure. We used optical tweezers to trap intracellular particles and to displace the cell nucleus. Two-photon fluorescence imaging of the manipulated cell can be performed simultaneously with trapping. The combination of techniques described here may help to solve a variety of problems in cell biology, such as positioning of organelles and the forces exerted by the cytoskeleton.

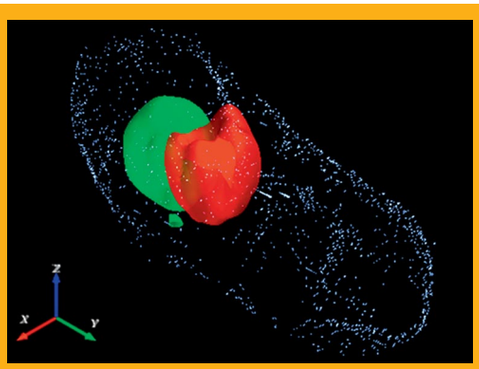


Three-dimensional representation of a cell where the nucleus was displaced using optical tweezers. The nucleus before the manipulation is displayed in red, and after the manipulation in green. The white dots show the cell volume.



## 1. Introduction

Since its beginnings, nonlinear microscopy [1] rapidly attracted interest, especially for its promising applications in biology. In particular, two-photon microscopy has been successfully applied in life sciences [2, 3] because of its advantages over confocal microscopy, such as a higher penetration depth and reduced photobleaching [4–6]. Moreover, since two-photon absorption is achieved only in regions of high photon density, the excitation is confined to a small volume around the focal point [7]. Therefore, two-photon microscopy is *intrinsically* confocal.

Exploiting this extremely confined excitation, multiphoton nanosurgery developed naturally along with nonlinear microscopy and allowed for local modification of structures in living cells with unprecedented accuracy [8, 9]. Although the exact physical mechanisms underlying the process are not yet fully understood, plasma formation likely plays a fundamental role [10–13]. However, experiments involving both two-photon imaging and multiphoton nanosurgery require careful optimization of the setup: damage of the sample may be induced by the ablation process, or during the image acquisition itself, especially when studying thin samples [14]. Laser microsurgery has

* Corresponding author: e-mail: maghelli@mpi-cbg.de

Journal of
BIOPHOTONICS



been used *in vivo* to ablate, e.g., the mitotic spindle [15–17], microtubules [18, 19], the cytoskeleton [20–22], neuronal processes [23] or axons [24].

Another technique that permits *in vivo* manipulation of cells and organelles is optical tweezers [25]. With the use of optical tweezers it is possible to apply forces in the pN range to cellular organelles without damaging the cell, in order to study mechanical and viscoelastic properties of living specimens [26–33]. Therefore, expanding a nonlinear microscope and laser ablation setup to include optical tweezers results in a versatile instrument capable of manipulating cells, both by applying forces and by modifying cellular structures. Moreover, the effects of such manipulations can be detected with high temporal resolution and spatial precision.

In this paper we present a combined system consisting of a two-photon microscope, a laser ablation module, and optical tweezers. We optimized and tested the setup on the fission yeast *Schizosaccharomyces pombe*, a model organism commonly used in cell biology.

## 2. Experimental Setup

### 2.1 Microscope

The setup (Figure 1) used was a custom-built upright microscope, consisting of an imaging system (Section 2.3), an ablation system (Section 2.5), and a trapping system (Section 2.6). The sample can be positioned by means of a coarse *xy* stage, based on mechanic translators (OWIS KT90 and HV100 for the *xy* and *z* directions, respectively) coupled to stepper motors (Trinamic PANdrive PD-013-42), and a 3D piezoelectric actuator (Physik Instrumente PI M.A.R.S.). Transmitted-light inspection of the sample is possible using a CCD camera (Pikelink PL-A653). All the mechanical hardware was either custom-built or commercially available (Thorlabs Inc.).

The setup can be used either with a high numerical aperture objective (Zeiss Plan-Apochromat 100x/1.40 Oil Ph3) or a water dipping objective (Zeiss W Plan-Apochromat 63x/1.0 VIS-IR). When used with the high numerical aperture objective, the sample was mounted in a sealed chamber, and an automatic perfusion system was used. The temperature of the sample was controlled by a Peltier controller and a thermoelectric element (Supercool TC-14-PR-59).

### 2.2 Laser sources

The laser source used to excite two-photon fluorescence and to perform ablation was a femtosecond Titanium-Sapphire (Ti : Sa) laser (Coherent Chameleon XR) with a nominal pulse width of 140 fs and a repetition rate of 90 MHz. The power at the objective back aperture during imaging was around 6 mW, and was increased to around 200 mW during ablation. For simultaneous excitation of the green fluorescent protein (GFP) and ablation, the laser was tuned to $\lambda = 895$ nm. At this wavelength, the objective has a transmission of around 50%, therefore, the power in the sample plane was around 3 mW and 100 mW during imaging and ablation, respectively. For optical trapping a continuous wave (CW)

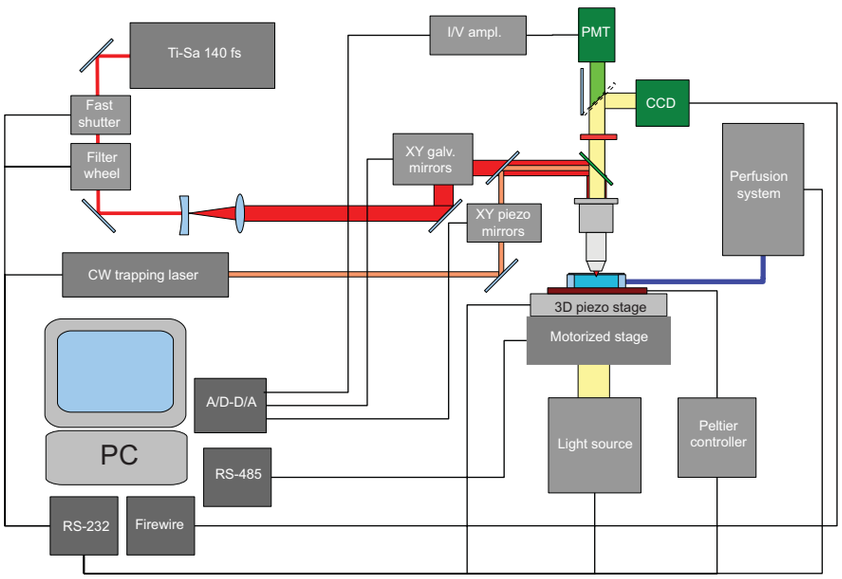


**Figure 1** (online colour at: www.biophotonics-journal.org) Microscope setup.

 

laser (Sacher Lasertechnik, external cavity Littrow system Tiger) tuned to $\lambda = 970$ nm was used. The transmission of the objective at this wavelength is around 45%, and the power at the sample plane during trapping was around 80 mW.

## 2.3 Imaging system

Laser radiation emitted from the Ti:Sa laser was expanded using a Galilean telescope with a magnification factor of 4. Optionally, a prism-based prechirper could be inserted in the beam path to compensate for the pulse broadening. The laser beam was then directed to two galvanometer scanning mirrors (GSI Lumonics VM500C) controlled by a closed-loop driver (GSI Lumonics MiniSAX). The beam was then focused onto the back focal plane, which is conjugate with the objective primary focal plane in the sample. The diameter of the beam at the objective back aperture was around 5 mm ($1/e^2$), resulting in a filling factor of around 1. The primary dichroic mirror of the microscope (Chroma Technology Corporation 650 dcspxr) separated the near-infrared excitation wavelengths from the emitted visible fluorescence.

## 2.4 Detection system

The fluorescence emission, collected by the objective, passed the primary dichroic mirror, an IR-blocking filter (AHF Analysentechnik HC 750/SP), an emission filter (Chroma Technology ET525/50 for GFP observations), and was finally detected by a photomultiplier (Hamamatsu, H9305-01). The photocurrent was converted to a voltage signal by a low-noise current preamplifier (Stanford Research SR570), and was digitized using a 16-bit A/D card (National Instruments PCI-6259).

Simultaneous two-color imaging was achieved by splitting the fluorescence emission with a dichroic mirror (Chroma Technology Corporation T560lpxr) and detecting the two channels using two photomultiplier tubes of the same type (Hamamatsu, H9305-01).

## 2.5 Ablation system

Laser ablation, performed during the continuous acquisition of a $z$-stack, was achieved by increasing the power of the Ti:Sa laser while scanning the beam over a user-defined region of interest (ROI). The time delay necessary to automatically reconfigure the optics to perform the ablation, and continue the ongoing stack acquisition, was around one second.

The ablation region could be defined by selecting an arbitrary shaped ROI on any plane of the stack being acquired. Each plane of the stack was displayed as a separate image on the screen using its original pixel size, i.e., each pixel of the image was reported as one pixel on the screen. To perform single point ablation, the software continuously scanned the stack until the user started the ablation subroutine. The acquisition continued until the laser beam reached the point on the sample that was designated for ablation. The fast shutter controlling the laser was closed and the galvanometer mirrors stopped. The computer then increased the power of the laser by rotating a filter wheel and exposed the sample for a defined exposure time. The filter wheel was brought back to its previous position, the shutter opened, and the image acquisition continued.

## 2.6 Optical tweezers

The CW laser beam was expanded using a 5× Galilean telescope, deflected by two piezoelectric mirrors (Physik Instrumente S-226), and coupled to the objective by a dichroic mirror (Chroma Technology z980bcm-sp). The piezoelectric mirrors were in a conjugate plane with the objective back focal plane. The beam diameter at the objective back aperture was around 10 mm (at $1/e^2$), resulting in a filling factor of around 2.

## 2.7 Perfusion system

The automatic perfusion system consisted of three solenoid valves. Two valves were connected to two inlets of a custom-built sealed sample chamber, while the third one controlled the outlet. All the valves were controlled by the computer, which was programmed to automatically open and close the valves for defined time intervals. This system was used to exchange the liquid medium contained in the chamber, e.g., to deliver or wash out a drug.

## 2.8 Software

The microscope was controlled by software written in Labview (National Instruments Labview v 8.5). The signal from the photomultiplier was digitized with 16-bit accuracy, displayed and stored as 8-bit monochrome TIFF images. The program controlled

Journal of
BIOPHOTONICS



all the main functions of the setup, including the coarse and fine sample positioning and focusing. This allowed the user to remotely operate the setup using a network connection, leaving the setup in an isolated room to minimize ambient light pickups and vibrations.

### 2.9 Sample preparation

Two strains of fission yeast were used: SV54 (*GFP-atb2*$^+$ *cut11-GFP sid4-GFP*, by Sven K. Vogel) and NK006 (*h*$^+$ *leu1 ura4 klp5::ura4*$^+$ *kan*$^r$*-nmtP3-GFP atb2*$^+$, kindly provided by Takashi Toda). The cells were grown on Edinburgh Minimal Medium (EMM) agar plates with appropriate supplements at 30 °C. The nmt1 promoter was repressed by the addition of 20 μM thiamine. For imaging, GFP expression was only partially repressed by adding 2 μM thiamine. Before imaging the cells were grown overnight (14–16 hours) in liquid EMM with appropriate supplements at 25 °C. For microscopy, the cells were resuspended in liquid EMM with appropriate supplements and transferred to a 22 × 22 mm microscope coverslip (0.17 mm thick) coated with 3 μl of 2 mg/ml lectin BS-1 (Sigma-Aldrich) in PBS. The coverslip was sealed with silicon in a custom-built perfusion chamber, filled with liquid EMM. During imaging, the temperature of the sample chamber was kept at 25 °C. For micromanipulation using optical tweezers, the microtubules were depolymerized using MBC (Carbendazim, 97%, Sigma-Aldrich) at a final concentration of 25 μg/ml in liquid EMM.

## 3. Results and Discussion

### 3.1 Point spread function

To maximize the time resolution using a scanning microscope, it is desirable to acquire the smallest possible number of pixels. However, decreasing the number of acquired pixels, while keeping the scan area big enough to image the relevant portion of the sample, results in a loss of spatial resolution. One must, therefore, find the best compromise between a fast time resolution and good spatial resolution [34].

The three-dimensional resolving power of a laser scanning microscope depends on many factors, and a theoretical calculation is difficult because of the unknown optical properties of the sample. However, the spatial extent of the microscope's point spread function (PSF) can give an estimate of the optimal pixel size that should be used. To measure the PSF of the microscope, we acquired a $z$-stack of images of sub-resolution green fluorescent microspheres (Invitrogen, PS-Speck Microscope Point Source Kit, nominal diameter 175 ± 5 nm) using a voxel size of 50 × 50 × 50 nm. We calculated the PSF using Huygens Pro (Scientific Volume Imaging) on the acquired stack. The excitation wavelength was 900 nm, while the detection filter had a 50 nm spectral width centered at 525 nm.

The radial and axial resolution, taken as the standard deviation of the fitted Gaussian curve to the PSF radial and axial profiles, were 141 nm and 628 nm, respectively (Figure 2). To guarantee maximum resolution without oversampling, a pixel size smaller than the PSF size, divided by a factor of 2.3,

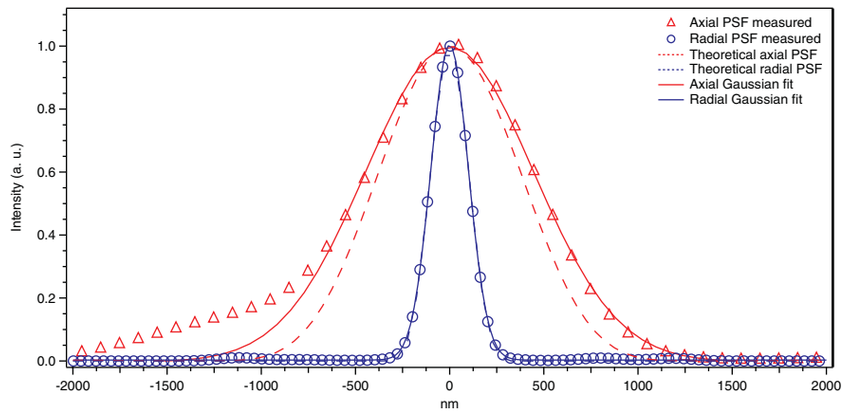


**Figure 2** (online colour at: www.biophotonics-journal.org) Measured axial (hollow red triangles) and radial (hollow blue circles) point spread function (PSF). For comparison, the theoretical curves, calculated as the square of the intensity profiles of the focused beam, are shown for the axial (dotted red line) and radial (dotted blue line) direction. The solid red and blue lines are Gaussian fits to the axial and radial measured PSF, respectively. The deviation from the theoretical prediction observed for the axial profile below −600 nm is due to the optical properties of the coverslip. Note that for the radial profile no significant deviation from the theoretical curve is observed.

 

should be used [34]. This corresponds to 61 nm in the *xy* plane, and a distance of 273 nm between planes. We decided to use a pixel size of 100 nm, and a minimum distance of 500 nm between adjacent planes when acquiring *z*-stacks as the best compromise between sampling accuracy and time resolution.

### *3.2 Accuracy of beam positioning*

To measure the accuracy of beam positioning when targeting a pixel for ablation, a series of single point bleaching was performed on a fluorescent polymer. Overshoot was typically observed when the system stopped the beam on the pixel targeted for ablation (Figure 3a). At a fixed magnification, the overshoot was observed only in the fast scan direction and depended on the pixel dwell time. The fitted function (Figure 3b) was used in the program controlling the ablation subroutine to correct for the overshoot. The resulting positioning accuracy after overshoot correction was $0.6 \pm 0.8$ pixel (mean $\pm$ standard error on the mean).

### *3.3 Long-term imaging*

When observing a sample for an extended period of time using laser scanning microscopy, the repeated irradiation could cause photodamage and, therefore, induce artifacts. In particular, if a high spatial and temporal resolution is required, it is important to illuminate the sample as much as possible, yet avoiding damage.

The intensity threshold at which photodamage sets in depends on the sample's optical properties at the wavelength used for illumination, the chemical environment, and the pulse width and repetition rate if nonlinear processes are exploited [35, 36]. To test the photodamage induced in the cells by our two-photon setup, we ran a long-term acquisition lasting for 5 hours, during which time the sample was continuously scanned. The results are shown in Figure 4.

The images were taken at $\lambda = 895$ nm, with an estimated average power at the sample plane of 3 mW and a pixel size of 100 nm, as described in Section 3.1. Each image is a maximum intensity projection of 10 planes, taken 500 nm apart. A single stack required 15 s, which was followed by the acquisition of a new stack. Thus, the sample was continuously irradiated during the whole acquisition. The analysis of the fluorescence signal integrated over the scanned area as a function of time showed no bleaching (Figure 4b). More importantly, during the 5-hour acquisition time the cells proceeded through the cell cycle. This suggests that the imaging did not induce significant photodamage.

### *3.4 Laser ablation*

In our setup, ablation was performed by increasing the power of the Ti:Sa laser used for imaging, while scanning the beam over a user-defined region of interest (ROI). Typically, the laser power in the sample plane during ablation was around 100 mW (see Section 2.2), with a pulse energy of around 1 nJ and exposure times ranging from 20 to 30 ms for interphase microtubules, and up to 50 ms for a larger structure, e.g., the mitotic spindle. Since the excitation is tightly confined to a small volume around the focal point, the ablation is three-dimensional, as seen in Figure 5a. Note that the user defined ROI can have an arbitrary shape.

The ablation setup was tested on interphase microtubules (Figure 5b), the mitotic spindle (Figure 5c), and a microtubule bundle during the sexual part of the yeast life cycle, namely meiotic prophase (Figure 5d). In each case, the cell did not show any additional sign of damage, except the locally induced ablation. In Figure 5b, the microtubule bundle was clearly cut: while the fragment closer to the cell end depolymerized and faded, the fragment closer to the nucleus shortened but later started growing again. As shown in Figure 5c, the spindle was cut into two fragments. The movement of the spindle poles toward each other after ablation shows that the spindle is under compression, and that the force for the spindle elongation is generated in the spindle itself [16]. In Figure 5d, the microtubule bundle trailing behind the spindle pole body was cut while the spindle pole body was moving downward. After ablation, the spindle pole body continued to move downward. This shows that microtubules pull and not push on the spindle pole body during meiotic prophase [37].

The lateral extension of the ablated region was estimated by severing a bright structure, such as the mitotic spindle, and plotting an intensity profile, as shown in Figure 5e–f. The region of decreased fluorescence had a maximum width of 1 μm. Since the structure was clearly severed, and the observed decrease of fluorescence resulted both from molecules that were ablated and molecules that were only photobleached, we conclude that the actual lateral extension of the ablation spot was less than 1 μm. Fitting a Gaussian curve to the data in Figure 5f, gave a value of 0.38 μm for the half-width of the ablation spot (not shown).

Contrary to the symmetric cutting of the spindle (Figure 5c), asymmetric cutting can be used to generate cells without a nucleus with high efficiency. Similar cell anucleation was shown by Raabe *et al.* [38] using a picosecond pulsed laser emitting at $\lambda = 405$ nm. Anucleate cells can be used to study cytoskeleton in a nucleus-free environment, as well as the role of the nucleus in cellular functions.

Journal of
BIOPHOTONICS



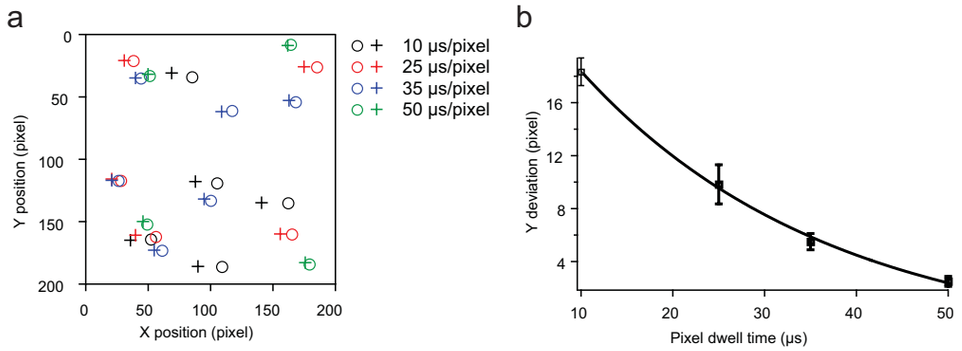


**Figure 3** (online colour at: www.biophotonics-journal.org) Overshoot is observed when selecting a pixel for ablation (a). The crosses represent the selected pixel, the circles the actually observed ablation locations. The deviation from the target (in pixels, error bars represent the standard error on the mean) is a function of the pixel dwell time (b). The fitted function is introduced in the software controlling the setup to correct for the overshoot.

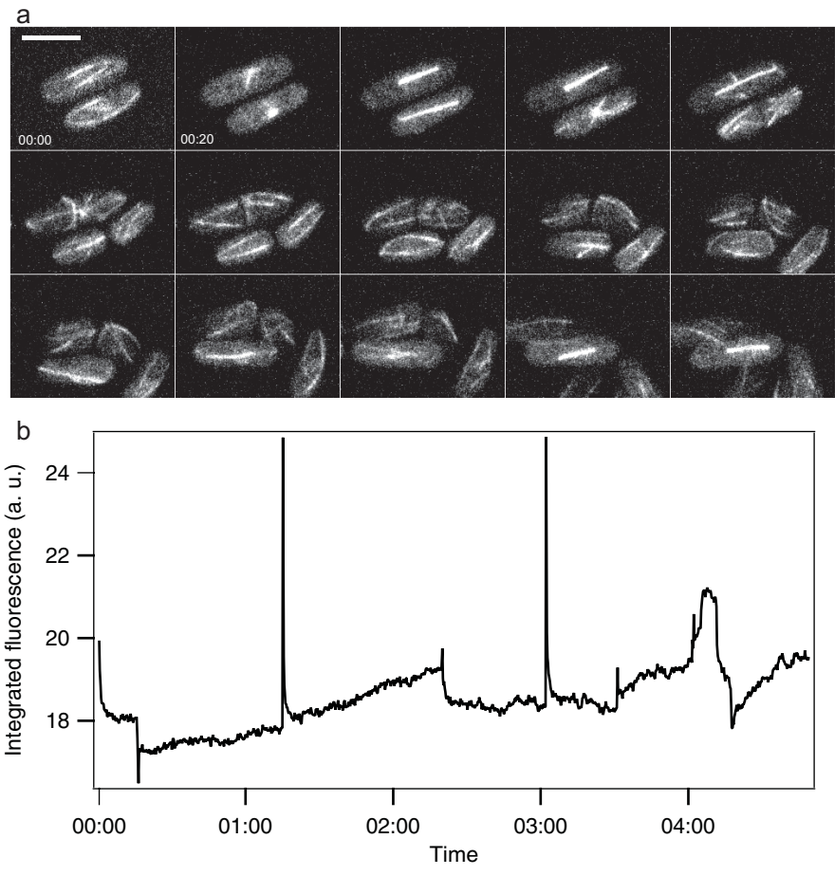


**Figure 4** Long-term imaging (a) and integrated fluorescence (b) of NK006 cells expressing GFP-tubulin. The sample was scanned continuously; the time interval between the shown frames is 20 min. Scale bar is 5 µm. The sharp peaks observed in (b) are due to refocusing during the image acquisition.

## *3.5 Ablation efficiency*

When irradiating cellular structures, such as microtubules, the probability of cutting depends on the laser power in the sample plane and on the exposure time. Since the laser source used in our setup emitted at a constant power, the intensity in the sample plane was controlled by inserting neutral density filters in the beam path. The filters, however, only allowed for a coarse control of the intensity, therefore, we fine-tuned the ablation process by varying the exposure time. Figure 6 shows the outcomes of irradiation of interphase microtubules as a function of the exposure time. Using an exposure time of

 

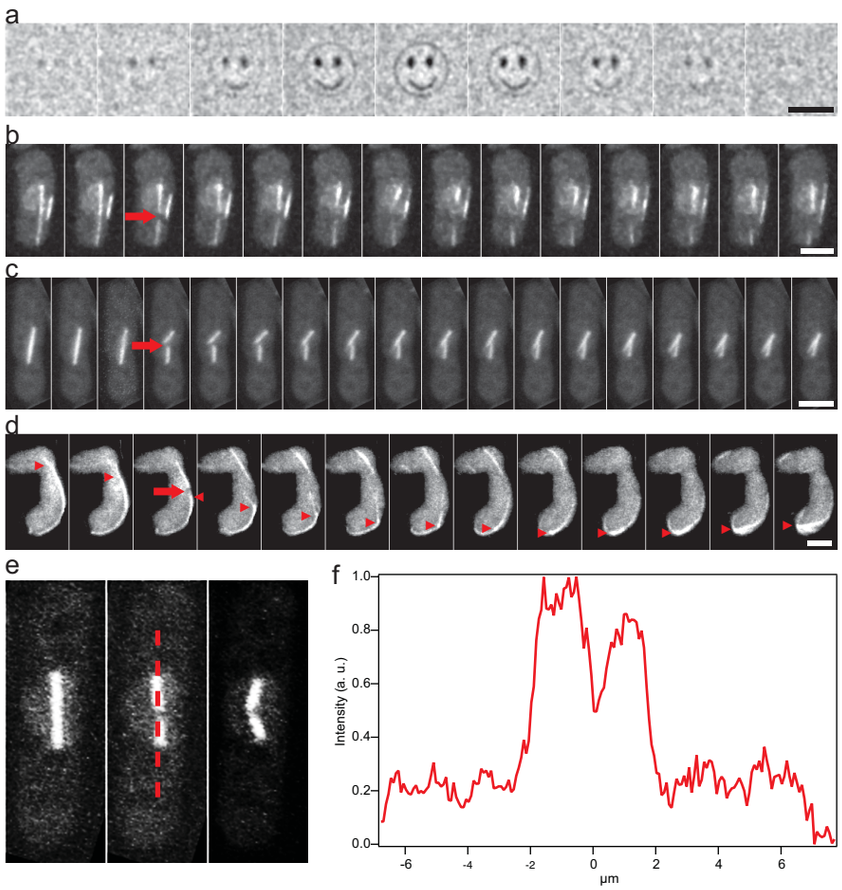


**Figure 5** (online colour at: www.biophotonics-journal.org) Three-dimensional bleaching of a fluorescent polymer (a): each image was taken on the same area, at a different focal height. The distance between two adjacent planes was 500 nm. Ablation of different cytoskeleton structures: an interphase microtubule bundle (b), the mitotic spindle (c), and a meiotic microtubule bundle (d). The red arrows mark the ablation point, the red triangles the position of the spindle pole body. Images show a single plane (b), or maximum intensity projection of a stack of 10 (c) or 12 (d) planes, taken 500 nm apart. The time interval between two separate frames was 1.75 s (b), 15 s (c) or 11 s (d). The intensity profile plotted in (f) was obtained from the profile marked in (e). The extension of the ablation region was smaller than 1 µm. Scale bars are 5 µm (a) and 3 µm (b–d). Sample in (d) by Sven K. Vogel.

10 ms mainly resulted in bleaching of the microtubules (78%), while increasing the exposure time to 20 and 30 ms resulted in a cutting efficiency of 50% and 69%, respectively. Further increasing the exposure time produced only a minor increase of the ablation efficiency (to 72%), with some cells dying as a consequence of the ablation (11%). We concluded that, using an intensity of around 100 mW in the sample plane, the optimal exposure time to cut interphase microtubules was around 20 to 30 ms.

## *3.6 Optical tweezers*

To trap micrometer-sized objects inside a living cell, we used a CW laser diode emitting at $\lambda = 970$ nm, focused by the microscope's objective. We chose this wavelength to minimize the photodamage, since this wavelength was found to be the least harmful for living bacteria in the range of $\lambda = 790$–$1064$ nm [39]. A potential well was generated inside the cell near the focus of the laser beam, allowing trapping of a particle with a refractive index higher than that of the cytoplasm, as shown in Figure 7a.

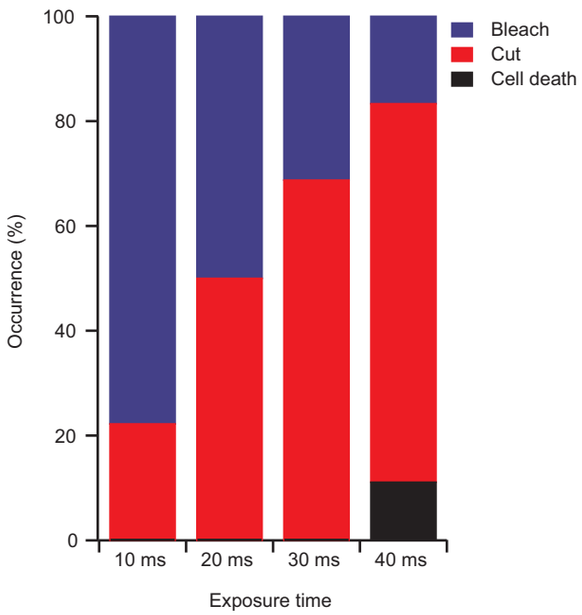


**Figure 6** (online colour at: www.biophotonics-journal.org) Irradiating an interphase microtubule can result in bleaching, cutting or cell death, depending on the exposure time.

Journal of
BIOPHOTONICS



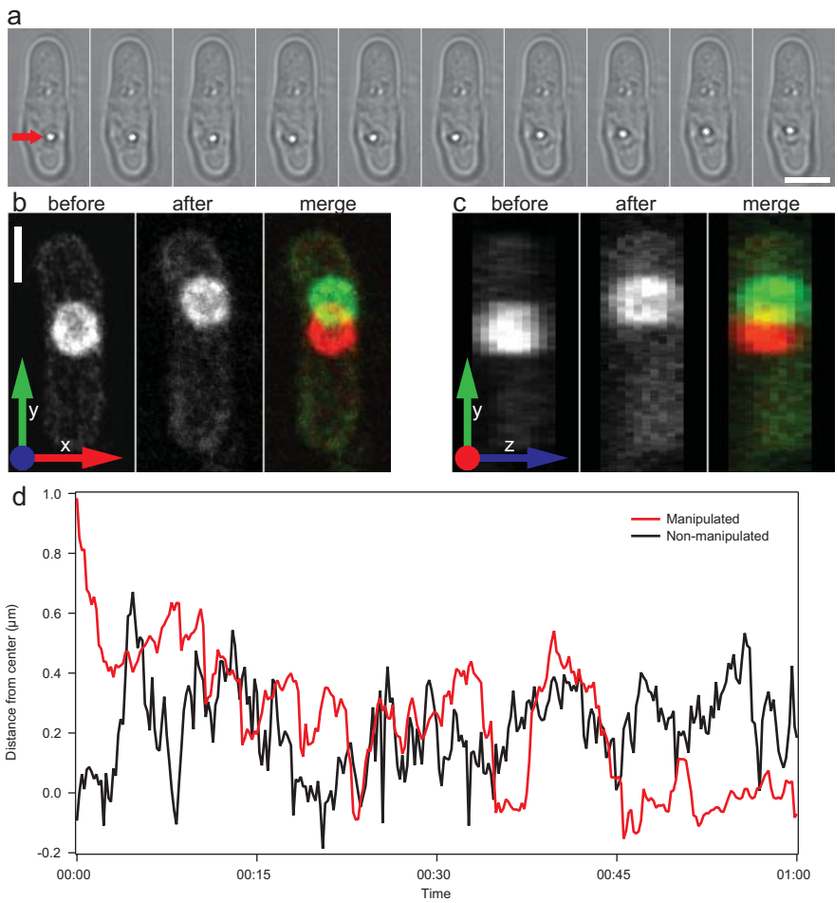


**Figure 7** (online colour at: www.biophotonics-journal.org) Transmitted light images of a trapped particle (red arrow) moved inside a living cell (a). Two-photon microscopy of a manipulated cell where the nucleus was displaced using optical tweezers (b–c): the cell is shown before (left) and after the manipulation (middle). The image on the right is a color merge of the previous two images. Projecting the dataset from (b) on an orthogonal plane (c) shows the three-dimensional displacement of the nucleus. Tracking of the nucleus after displacement (d, red). For comparison, tracking of a non-manipulated nucleus is also shown (black). Time between frames in (a) is 5 s. Scale bars are 3 μm.

The trapped particle could be used to apply forces on cell organelles, e.g., the nucleus, that could be displaced from its original position [27]. Figure 7a shows a cell in which a particle, most likely a lipid droplet, was trapped inside the cytoplasm and was used to displace the nucleus (not visible in the transmitted-light images). The particle trapped near the focus of the trapping beam (red arrow) was moved laterally inside the cell and simultaneously dragged upward towards the nucleus. Figure 7b–c shows the nucleus, labeled with Cut11-GFP, displaced by the applied force. The cell was treated with MBC to depolymerize the microtubules before moving the nucleus (see Section 2.9). Although displacement of cell organelles is possible without perturbing the microtubules [26], the MBC treatment increased the efficiency of the displacement process, since microtubules can exert forces on the organelles, and therefore interfere with the displacement.

To test whether the manipulation process induced damage to the cell, we washed out MBC, allowing the microtubules to polymerize, and started a long-term acquisition immediately after displacing the nucleus. The manipulated cell showed dynamic microtubule bundles, similar to a non-manipulated cell (not shown). Moreover, the tracking of the nucleus, performed using the *Spot Tracker* plugin for ImageJ [40] and validated manually, showed that the nucleus returned to the cell center [27, 41, 42], (Figure 7d, red). These results suggest that the manipulation process did not cause damage. The trajectory of the displaced nucleus showed a net movement toward the cell center, with fluctuations of amplitude comparable to those of the nuclear position in a non-manipulated cell (Figure 7d, black). The optically induced displacement of the nucleus (about 1 μm) was larger than these fluctuations (peak-to-peak amplitude of about 0.5 μm).

### *3.7 Simultaneous optical manipulation and imaging*

A novel feature of our setup, compared to the previously published ones [26, 19], is the simultaneous acquisition of two-photon fluorescence while applying optical forces in a living cell (Figure 8). Obser-

 

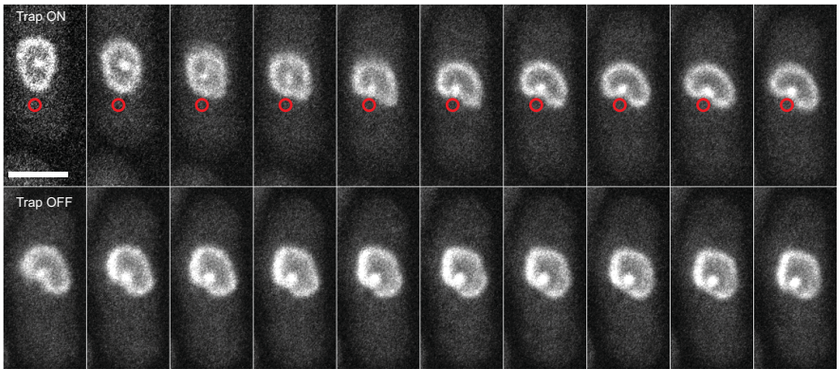


**Figure 8** (online colour at: www.biophotonics-journal.org) Two-photon fluorescence of a cell labeled with Cut11-GFP and Sid4-GFP during optical trapping. The trap, marked with the red circles, is fixed with respect to the scan area, while the sample is translated toward the trap. In the upper row, the nucleus is clearly deformed as the trap interacts with the nuclear membrane. Switching off the trap (lower row) results in spontaneous reshaping of the nucleus close to its original, nearly spherical form. Scale bar, 3 μm, time between frames is 20 s.

ving a structure while displacing it guarantees a higher efficiency of displacement in comparison to "blind" methods. Moreover, studying the dynamics of the displacement process and the nuclear morphology during the interaction with the optical trap, can provide additional information about the nuclear centering mechanism.

## 4. Conclusion

We have presented a custom-built two-photon microscope and laser ablation setup combined with optical tweezers. We achieved bleaching- and photodamage-free continuous imaging of living cells over a period of 5 hours. We performed precise *in vivo* ablation of sub-cellular structures, such as microtubules or the mitotic spindle, without compromising cell viability. Finally, we were able to trap cytoplasmic particles inside living cells, and use them to displace the nucleus, while simultaneously observing the fluorescence of the labeled nuclear membrane.

In conclusion, two-photon microscopy, in combination with femtosecond near-infrared laser ablation, is an efficient and non-invasive technique that can be used to locally perturb cellular organization and observe the response of the biological system over an extended period of time. The implementation of optical tweezers, using a laser emitting at a wavelength where photodamage is minimal, allows manipulation of the cell without inducing artifacts.

This versatile setup can be used to study fundamental problems in cell biology, such as the force balance in the cytoskeleton [43]: forces acting on the mitotic spindle [16], forces driving the meiotic nuclear oscillation [37], and forces responsible for nuclear centering [27].

**Acknowledgments** We thank Hartmut Wolf and the MPI-CBG mechanical workshop for manufacturing some of the components of the microscope; Sven K. Vogel and Takashi Toda for the yeast strains; Leonardo Sacconi, Francesco Pavone, Volker Türck, Isabel Raabe, Yvonne Caldarelli, Jan Peychl, Britta Schroth-Diez, Matt Boes, and the members of the Tolić-Nørrelykke group for technical support, discussions, and comments on the manuscript; and Judith Nicholls for proof-reading.

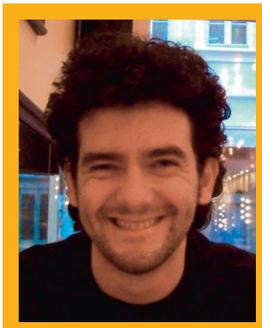

**Nicola Maghelli** received his B. Sc. in Physics in 2000 from the University of Pisa, Italy, in the group of Prof. Maria Allegrini. He completed his Ph. D. in 2005 at the University of Ulm, Germany, working in the laboratory of Prof. Othmar Marti. Currently he is working as a post-doc in the group of Iva M. Tolić-Nørrelykke at the Max Planck Institute of Molecular Cell Biology and Genetics in Dresden, Germany.

**Iva M. Tolić-Nørrelykke** obtained her Ph.D. in 2002 from the University of Zagreb, Croatia. She did her thesis work with Prof. Ning Wang at the Harvard School of Public Health in Boston, USA, and with Prof. Nenad Trinajstić at the Rugjer Bošković Insitute in Zagreb. In 2002 she moved to the Niels

Bohr Institute in Copenhagen, Denmark, to work as a post-doc with Profs. Lene Oddershede and Kirstine Berg-Sørensen. From 2003 until 2004 she worked at LENS – European Laboratory for Non-Linear Spectroscopy in Florence, Italy, as a post-doc in the laboratory of Prof. Francesco Pavone. Currently she is a group leader at the Max Planck Institute of Molecular Cell Biology and Genetics in Dresden, Germany.

## References

[1] W. Denk, J. H. Strickler, and W. W. Webb, Two-photon laser scanning fluorescence microscopy, Science **248**, 73–76 (1990).
[2] W. Denk and K. Svoboda, Photon upmanship: why multiphoton imaging is more than a gimmick, Neuron **18**, 351–357 (1997).
[3] K. König, Multiphoton microscopy in life sciences, Journal of Microscopy **200**, 83–104 (2000).
[4] P. Theer and W. Denk, On the fundamental imaging-depth limit in two-photon microscopy. Journal of the Optical Society of America A: Image, Science and Vision **23**, 3139–3149 (2006).
[5] V. E. Centonze and J. G. White, Multiphoton excitation provides optical sections from deeper within scattering specimens than confocal imaging, Biophysical Journal **75**, 2015–2024 (1998).
[6] P. P. Mondal and A. Diaspro, Reduction of higher-order photobleaching in two-photon excitation microscopy, Physical Review. E, Statistical, nonlinear, and soft matter physics **75**, (2007).
[7] A. Diaspro, P. Bianchini, G. Vicidomini, M. Faretta, P. Ramoino, and C. Usai, Multi-photon excitation microscopy, BioMedical Engineering OnLine **5**, 36 (2006).
[8] W. Watanabe, N. Arakawa, S. Matsunaga, T. Higashi, K. Fukui, K. Isobe, and K. Itoh, Femtosecond laser disruption of subcellular organelles in a living cell, Optics Express **12**(18), 4203–4213 (2004).
[9] K. König, I. Riemann, P. Fischer, and K. J. Halbhuber, Intracellular nanosurgery with near infrared femtosecond laser pulses, Cellular and Molecular Biology, **45**, 195–201 (1999).
[10] V. Venugopalan, A. Guerra, K. Nahen, and A. Vogel, Role of laser-induced plasma formation in pulsed cellular microsurgery and micromanipulation, Physical Review Letters, **88**, (2002).
[11] A. Vogel, N. Linz, S. Freidank, and G. Paltauf, Femtosecond-laser-induced nanocavitation in water: implications for optical breakdown threshold and cell surgery, Physical Review Letters **100**, (2008).
[12] A. Vogel, J. Noack, G. Hüttman, and G. Paltauf, Mechanisms of femtosecond laser nanosurgery of cells and tissues, Applied Physics B: Lasers and Optics, **81**, 1015–1047 (2005).
[13] A. Heisterkamp, I. Z. Maxwell, E. Mazur, J. M. Underwood, J. A. Nickerson, S. Kumar, and D. E. Ingber, Pulse energy dependence of subcellular dissection by femtosecond laser pulses, Optics Express, **13**, 3690–3696 (2005).
[14] G. H. Patterson and D. W. Piston, Photobleaching in two-photon excitation microscopy, Biophysical Journal **78**, 2159–2162 (2000).
[15] J. R. Aist and M. W. Berns, Mechanics of chromosome separation during mitosis in fusarium (fungi imperfecti): new evidence from ultrastructural and laser microbeam experiments, The Journal of Cell Biology **91**, 446–458 (1981).
[16] I. M. Tolić-Nørrelykke, L. Sacconi, G. Thon, and F. S. Pavone, Positioning and elongation of the fission yeast spindle by microtubule-based pushing, Current Biology **14**, 1181–1186 (2004).
[17] A. Khodjakov, S. La Terra, and F. Chang, Laser microsurgery in fission yeast; role of the mitotic spindle midzone in anaphase b, Current Biology **14**, 1330–1340 (2004).
[18] E. L. Botvinick, V. Venugopalan, J. V. Shah, L. H. Liaw, and M. W. Berns, Controlled ablation of microtubules using a picosecond laser, Biophysical Journal **87**, 4203–4212 (2004).
[19] L. Sacconi, I. M. Tolić-Nørrelykke, R. Antolini, and F. S. Pavone, Combined intracellular three-dimensional imaging and selective nanosurgery by a nonlinear microscope, Journal of Biomedical Optics **10**(1), (2005).
[20] S. Kumar, I. Z. Maxwell, A. Heisterkamp, T. R. Polte, T. P. Lele, M. Salanga, E. Mazur, and D. E. Ingber, Viscoelastic retraction of single living stress fibers and its impact on cell shape, cytoskeletal organization, and extracellular matrix mechanics, Biophysical Journal **90**, 3762–3773 (2006).
[21] J. Colombelli, E. G. Reynaud, and E. H. Stelzer, Subcellular nanosurgery with a pulsed subnanosecond uv-a laser, Medical Laser Application **20**, 217–222 (2005).
[22] J. Colombelli, E. G. Reynaud, J. Rietdorf, R. Pepperkok, and E. H. Stelzer, In vivo selective cytoskeleton dynamics quantification in interphase cells induced by pulsed ultraviolet laser nanosurgery, Traffic **6**, 1093–1102 (2005).
[23] L. Sacconi, R. P. O'Connor, A. Jasaitis, A. Masi, M. Buffelli, and F. S. Pavone, In vivo multiphoton nanosurgery on cortical neurons, Journal of Biomedical Optics **12**(5), (2007).
[24] S. X. Guo, F. Bourgeois, T. Chokshi, N. J. Durr, M. A. Hilliard, N. Chronis, and A. B. Yakar, Femtosecond laser nanoaxotomy lab-on-a-chip for in vivo nerve regeneration studies, Nature Methods **5**, 531–533 (2008).
[25] A. Ashkin and J. M. Dziedzic, Optical levitation by radiation pressure, Applied Physics Letters **19**(8), 283–285 (1971).
[26] L. Sacconi, I. M. Tolić-Nørrelykke, C. Stringari, R. Antolini, and F. S. Pavone, Optical micromanipulations inside yeast cells, Applied Optics **44**, 2001–2007 (2005).
[27] I. M. Tolić-Nørrelykke, L. Sacconi, C. Stringari, I. Raabe, and F. S. Pavone, Nuclear and division-plane

 

positioning revealed by optical micromanipulation, Current Biology **15**, 1212–1216 (2005).
[28] I. M. Tolić-Nørrelykke, E. L. Munteanu, G. Thon, L. Oddershede, and Berg-Sørensen, Anomalous diffusion in living yeast cells, Physical Review Letters **93**(7), (2004).
[29] S. Grabski, X. G. Xie, J. F. Holland, and M. Schindler, Lipids trigger changes in the elasticity of the cytoskeleton in plant cells: a cell optical displacement assay for live cell measurements, Journal of Cell Biology **126**, 713–726 (1994).
[30] G. Leitz, E. Schnepf, and K. O. Greulich, Micromanipulation of statoliths in gravity-sensing chara rhizoids by optical tweezers, Planta **197**, 278–288 (1995).
[31] S. Bayoudh, M. Mehta, H. Rubinsztein-Dunlop, N. R. Heckenberg, and C. Critchley, Micromanipulation of chloroplasts using optical tweezers, Journal of Microscopy **203**, 214–222 (2001).
[32] A. Holzinger, S. Monajembashi, K. O. Greulich, and U. Lütz-Meindl, Impairment of cytoskeleton-dependent vesicle and organelle translocation in green algae: combined use of a microfocused infrared laser as microbeam and optical tweezers, Journal of Microscopy **208**, 77–83 (2002).
[33] T. Ketelaar, C. Faivre-Moskalenko, J. J. Esseling, N. C. de Ruijter, C. S. Grierson, M. Dogterom, and A. M. Emons, Positioning of nuclei in arabidopsis root hairs: an actin-regulated process of tip growth, The Plant cell **14**, 2941–2955 (2002).
[34] J. Pawley, Handbook of Biological Confocal Microscopy. Springer, August 2006.
[35] A. Hopt and E. Neher, Highly nonlinear photodamage in two-photon fluorescence microscopy, Biophysical Journal **80**, 2029–2036 (2001).
[36] S. Tang, T. B. Krasieva, Z. Chen, G. Tempea, and B. J. Tromberg, Effect of pulse duration on two-photon excited fluorescence and second harmonic generation in nonlinear optical microscopy, Journal of Biomedical Optics **11**(2), (2006).
[37] S. K. Vogel, N. Pavin, N. Maghelli, F. Jülicher, and I. M. Tolić-Nørrelykke, Self-organization of dynein motors generates meiotic nuclear oscillations, Submitted (2008).
[38] I. Raabe, S. K. Vogel, J. Peychl, and I. M. Tolić-Nørrelykke, Intracellular microsurgery and cell anucleation using a picosecond laser, Submitted (2008).
[39] K. C. Neuman, E. H. Chadd, G. F. Liou, K. Bergman, and S. M. Block, Characterization of photodamage to Escherichia coli in optical traps, Biophysical Journal **77**, 2856–2863 (1999).
[40] D. Sage, F. R. Neumann, F. Hediger, S. M. Gasser, and M. Unser, Automatic tracking of individual fluorescence particles: application to the study of chromosome dynamics, IEEE transactions on image processing: a publication of the IEEE Signal Processing Society **14**, 1372–1383 (2005).
[41] R. R. Daga, A. Yonetani, and F. Chang, Asymmetric microtubule pushing forces in nuclear centering, Current Biology **16**, 1544–1550 (2006).
[42] J. Howard, Elastic and damping forces generated by confined arrays of dynamic microtubules, Physical Biology **3**, 54–66 (2006).
[43] I. M. Tolić-Nørrelykke, Push-me-pull-you: how microtubules organize the cell interior, European Biophysics Journal, DOI 10. 1007/s00249-008-0321-0 (2008).